NANO LETTERS

2008
Vol. 8, No. 8
2283-2288

Enhanced Thermopower in PbSe Nanocrystal Quantum Dot Superlattices

Robert Y. Wang,[†] Joseph P. Feser,[†] Jong-Soo Lee,[‡,§] Dmitri V. Talapin,[*,‡,§] Rachel Segalman,[*,||] and Arun Majumdar[*,†,⊥]

Department of Mechanical Engineering, University of California, Berkeley, California 94720, The Molecular Foundry, Lawrence Berkeley National Laboratory, Berkeley, California 94720, Department of Chemistry, University of Chicago, Chicago, Illinois 60637, Department of Chemical Engineering, University of California, Berkeley, California 94720, and Department of Materials Science and Engineering, University of California, Berkeley, California 94720

Received April 5, 2008; Revised Manuscript Received June 6, 2008

ABSTRACT

We examine the effect of strong three-dimensional quantum confinement on the thermopower and electrical conductivity of PbSe nanocrystal superlattices. We show that for comparable carrier concentrations PbSe nanocrystal superlattices exhibit a substantial thermopower enhancement of several hundred microvolts per Kelvin relative to bulk PbSe. We also find that thermopower increases monotonically as the nanocrystal size decreases due to changes in carrier concentration. Lastly, we demonstrate that thermopower of PbSe nanocrystal solids can be tailored by charge-transfer doping.

Developing low-cost and efficient thermoelectric materials is a field of growing academic and technological interest.[1,2] The performance of a thermoelectric material can be evaluated by its thermoelectric figure of merit, $ZT = S^2\sigma T/k$, where S is the Seebeck coefficient (also known as thermopower), σ is the electrical conductivity, k is the thermal conductivity, and T is the absolute temperature. It was predicted recently that low-dimensional materials can provide large values of ZT.[3–5] Since then, several high-ZT nanostructured materials have been reported.[6–10] However, practical use of these materials is hampered by complicated and expensive synthesis techniques, such as molecular-beam epitaxy.[7] Although improvements in ZT for nanostructured materials have generally been attributed to reductions in thermal conductivity,[1,2] the unique electronic structure of low-dimensional materials can also have a strong impact on thermopower and charge transport.

Colloidal synthesis of monodisperse nanocrystals could offer a convenient route to low-cost and production-scalable low-dimensional thermoelectric materials. Moreover, chemical synthesis allows precise tuning of the nanocrystal size in the sub-10-nm range typically inaccessible for molecular-beam-epitaxy-grown quantum dots.[11] This opens up the possibility to explore thermoelectric properties of strongly quantum-confined materials. In this regime, the valence and conduction bands of a semiconductor collapse into well-separated discrete energy states,[2,12,13] which alters the fundamental properties of a semiconductor such as the electronic density of states (DOS) and band-gap energy.[2,12,13] Quantum confinement leads to sharp delta-function-like peaks in the DOS, which is predicted by Mahan and Sofo[14] to be the best possible electronic structure for a thermoelectric material. Recent calculations by Humphrey and Linke[15] predict that optimized nanostructured materials with a delta-function-like DOS can have ZT approaching 10 at room temperature. This exciting prediction originates from the fundamental difference between thermodynamics and transport in nanostructured materials as compared to bulk thermoelectric materials.[15] It is also anticipated that these materials will have advantageous thermal properties because the nanocrystal diameters are much smaller than the phonon mean free path ($\sim 10^{-7}$ to 10^{-8} m for crystalline materials at room temperature).[16,17] This causes a strong suppression of thermal conductivity due to phonon scattering at the nanocrystal boundaries.[18,19] In our work, this extreme regime is realized by using PbSe nanocrystal superlattices with varying nanocrystal sizes.

* Corresponding authors. E-mail: majumdar@me.berkeley.edu; segalman@berkeley.edu; dvtalapin@uchicago.edu.

† Department of Mechanical Engineering, University of California, Berkeley.

‡ The Molecular Foundry, Lawrence Berkeley National Laboratory.

§ Department of Chemistry, University of Chicago.

|| Department of Chemical Engineering, University of California, Berkeley.

⊥ Department of Materials Science and Engineering, University of California, Berkeley.

10.1021/nl8009704 CCC: $40.75
Published on Web 07/03/2008

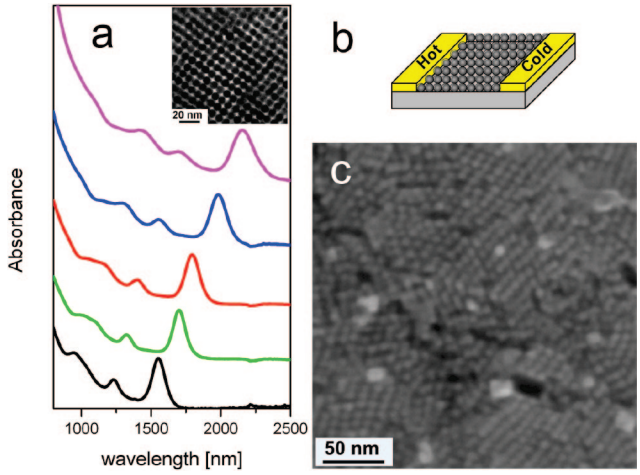

Figure 1. (a) Absorption spectra of PbSe nanocrystals dispersed in tetrachloroethylene. The diameters are 4.8 (black), 5.6 (green), 6.4 (red), 7.1 (blue), and 8.6 nm (pink). The electronic structure of PbSe depends on the particle size due to quantum confinement. The inset shows the transmission electron microscopy image of PbSe nanocrystals with diameter ~7.1 nm. (b) The measurement device consisted of a glass wafer with two Cr/Au electrodes. (c) Typical high-resolution scanning electron microscopy image of a conductive PbSe nanocrystal film used in this study.

Charge transport in an array of close-packed semiconductor nanocrystals separated by thin barriers can occur by hopping between quantum-confined orbitals with S and P symmetry.[20,21] To date, arrays of lead chalcogenide nanocrystals show the most promising charge transport properties. This is due to their monodispersity and eightfold degeneracy of 1S electron and hole states that allows good energy-level alignment between adjacent particles, leads to sharp peaks in the electronic DOS, and provides a very large number of electronic states available for charge transport.[22] The extraordinarily large static dielectric constant of PbSe ($\epsilon \sim 250$) brings down the charging energy and prevents Coulomb blockade in PbSe nanocrystal solids.[22,23] We demonstrated recently that engineering interparticle spacing allows tuning of the exchange coupling energy and can increase carrier mobility in self-assembled superlattices of PbSe nanocrystals by many orders of magnitude approaching >1 cm^2/Vs.[22] Ultimately, further increases of quantum-mechanical coupling between individual nanocrystals packed into a long-range ordered superlattice should lead to high-mobility Bloch transport through three-dimensional minibands.[24] Lastly, bulk lead chalcogenides are used widely in commercial thermoelectric devices due to the combination of S, σ, and k parameters naturally favoring large values of ZT.

PbSe nanocrystals of different size were synthesized by reacting lead oleate with tri-*n*-octylphosphine selenide in squalane in the presence of oleic acid capping ligands.[22] We varied the size of the nanocrystals from ~4.3 to ~8.6 nm while keeping the size distribution well below 10%. The narrow size distribution allows the resolution of the sharp excitonic features in the absorption spectra of the colloidal solutions and can also be seen in the transmission electron microscopy images (Figure 1a). Prior to nanocrystal film deposition, glass substrates were treated with hexamethyl disilazane to improve the wetting properties. Films of monodisperse PbSe nanocrystals were deposited by drop-casting hexane/octane (9:1 by volume) solutions on substrates with preformed parallel Cr/Au electrodes (Figure 1b). The resulting film thickness was generally 50−200 nm. The PbSe nanocrystals are initially coated with oleic acid ligands. After drop-casting, the oleic acid is removed by hydrazine treatment as described in ref 22 (**NOTE: hydrazine is toxic and should be handled using appropriate protective equipment to prevent contact with either the vapors or the liquid**). Hydrazine molecules replace oleic acid at the nanocrystal surface, which reduces the interparticle spacing from ~1.1 nm down to 0.4 nm and results in greatly improved electrical conductivity.[22] Hydrazine treatment does not change the nanocrystal's size and shape (Figure 1c); treated nanocrystal films possess characteristic excitonic features in the absorption spectrum.[22]

Unless stated otherwise, all nanocrystal superlattices were kept inside a dry-nitrogen glovebox during storage and measurements. Temperature gradients for the thermopower measurements were created with commercially available thermoelectric devices. Voltages and temperatures were measured with an Agilent 34401a voltmeter and thermocouples, respectively. The temperature gradient was modulated by varying the electrical current to the thermoelectric devices. After hydrazine treatment, the thermopower and conductivity of the nanocrystal film exhibited a strong time-dependence that asymptotes. We attribute this time-dependence to the changes in hydrazine concentration in the nanocrystal solid (vide infra). The length of this transience increased for smaller nanocrystal sizes and generally varied between 1 and 15 days. Unless indicated otherwise, the data presented is taken at the asymptote of this transience.

When a temperature gradient, ($|\Delta T| = 0-30$ K) is created across the nanocrystal film, an open circuit voltage V_{oc} proportional to the temperature gradient is observed (Figure 2a). The Seebeck coefficient is given by $-dV_{oc}/dT$ (e.g., a positive Seebeck coefficient implies that the cold region develops a higher potential than the hot region). The dependence on nanocrystal size for thermopower is shown in Figure 2b. As the nanocrystal size decreases from 8.6 to 4.8 nm, the thermopower increases from 700 to 1150 μV/K. The positive sign of thermopower indicates that transport in these films is p-type. A combination of electrical conductivity and field-effect transistor measurements provide insight into these thermopower results. Over the same nanocrystal size range, we observed a drop in electrical conductivity by about 1 order of magnitude (Figure 2c). Field-effect hole mobility was ~0.1 cm^2/V-s and no nanocrystal size dependence was observed (Figure S1 from Supporting Information). Using the mobility data, we can calculate the carrier concentration in our nanocrystal solids because $\sigma = ne\mu$, where μ is the mobility, e is the electron charge, and n is the carrier concentration. The carrier concentrations in Figure 2 are representative of the entire film volume. Simple estimates yield ~0.2 carriers/dot for the 8.6 nm nanocrystals and ~0.002 carriers/dot for the 4.3 nm nanocrystals. For comparable carrier concentrations, the PbSe nanocrystal film

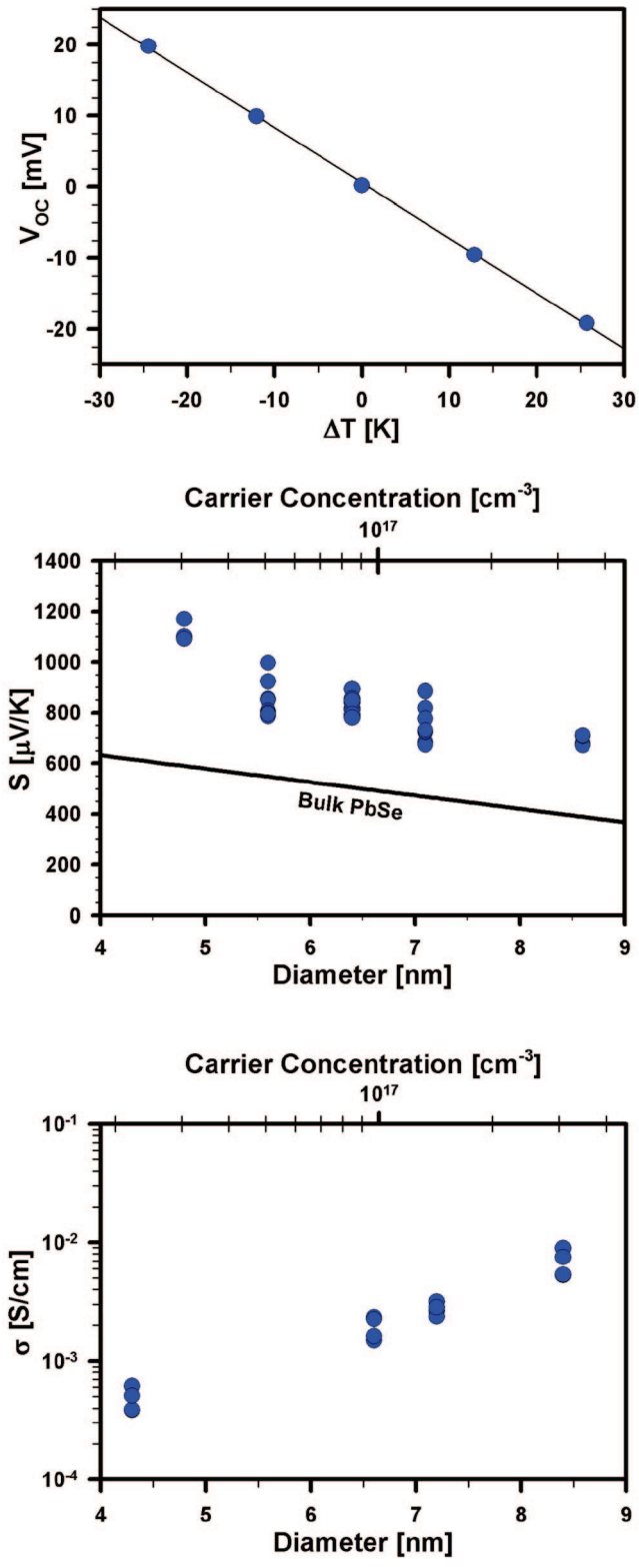

Figure 2. (a) Open circuit voltage, V_{oc}, generated in a 6.4-nm PbSe nanocrystal solid by a temperature gradient, ΔT, due to the Seebeck effect. (b) Nanocrystal size-dependence for thermopower. (c) Nanocrystal size-dependence for electrical conductivity. In both b and c, the approximate carrier concentration is indicated on the top axis (log scale). Because of uncertainties in mobility, there is an uncertainty factor of ~2 for the carrier concentration. The thermopower curve for bulk PbSe is taken from ref 25.

exhibits a significant thermopower enhancement of several hundred microvolts per Kelvin relative to bulk PbSe.[25] This

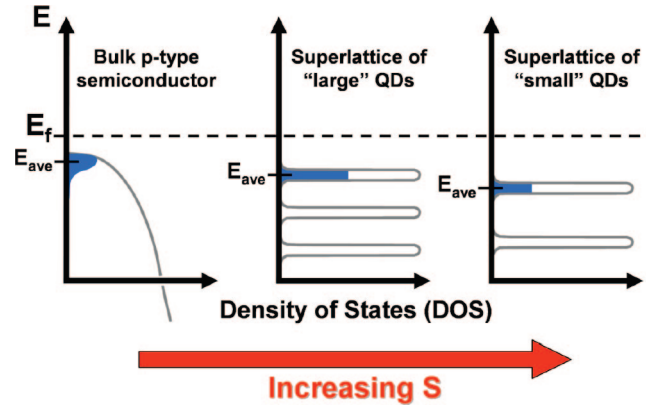

Figure 3. A mechanism that can qualitatively explain the size dependence of thermopower in the nanocrystal solids. The electronic density of states is represented by the gray lines. The carrier concentration is represented by the area of the blue region and the thermopower is approximately proportional to $E_f - E_{ave}$, where E_f and E_{ave} are the Fermi energy and average energy of conducting holes, respectively. See the text for more detail.

enhancement in thermopower is a signature of the sharper peaks in the nanocrystal solid DOS relative to the bulk DOS.

The thermopower is approximately proportional to the difference between the Fermi Energy (E_f) and average mobile carrier energy (E_{ave}). In a bulk material with parabolic bands, the Fermi−Dirac occupation function gives a wide distribution of carrier energies (shown schematically in Figure 3a). The DOS of zero-dimensional quantum dots differs dramatically from that of a bulk semiconductor (Figure 3b and c).[2,13,24] It has been predicted that thermoelectric power factor ($S^2\sigma$) can be enhanced greatly when the chemical potential is within a few kT's of the delta-function-like DOS of the ground state and/or one of the excited states.[14] Although we observe an enhanced thermopower, we do not observe an enhanced power factor due to low carrier mobility. Aside from enhanced thermopower, nanomaterials should also benefit from a relaxation in the Wiedemann−Franz law because it loses validity in materials with a delta-function-like DOS.[15] Relative to bulk materials, nanostructured materials can have an increased ratio of electrical conductivity to electronic thermal conductivity (k_e) yielding overall greater values of ZT.[15]

One possible explanation for the observed size dependence of thermopower and electrical conductivity originates in the size-dependent band gap of the nanocrystals. The peaks in the nanocrystal absorption spectra (Figure 1a) exhibit progressive blue-shift[12] for decreasing nanocrystal size. This is a signature of the energy band gap, E_g, increasing as the nanocrystal size decreases. Over the nanocrystal size range studied in this paper, the absorption peak changes by ~230 meV. Figure 3b and c illustrates the situation where $\Delta E_f \ll \Delta E_g$ for changes in nanocrystal size (where ΔE_f and ΔE_g are the changes in Fermi Energy and energy band gap, respectively). As the nanocrystal size decreases, the band edge moves away from the Fermi Energy, which results in an increased difference between E_f and E_{ave} (Figure 3b and c). Because thermopower is approximately proportional to $E_f - E_{ave}$, thermopower increases as the nanocrystal size

decreases. This process also results in changes of carrier concentration; larger carrier concentrations are obtained when E_f is near the band edge. As the nanocrystal size increases, the band edge moves closer to E_f. This causes the carrier concentration (and therefore the electrical conductivity) to increase. This explanation is further supported by the fact that mobility did not change with nanocrystal size, which implies that the observed changes in conductivity (Figure 2c) are due to variations in carrier concentration. Another plausible explanation for thermopower size dependence is alteration of the scattering mechanisms that occur in nanostructured materials, which can lead to carrier-energy filtering.[26]

In the case of PbSe quantum wells, the thermopower and electrical conductivity were found to oscillate with well thickness.[27] In contrast, we observe monotonic changes in thermopower and electrical conductivity. This paper reports the first thermopower measurements of solution-processed low-dimensional materials in the regime of strong quantum confinement. The observed size dependence creates opportunities to tune the thermopower in these materials.

Besides obvious interest to thermoelectric applications of nanocrystal solids, thermopower measurements are proven to be a very powerful technique in fundamental studies of electronic structure and doping of bulk materials. In particular, it can unambiguously point to the type of carriers responsible for charge transport and provide valuable information on the Fermi energy under particular experimental conditions. Because thermopower is measured under open-circuit conditions, it is not affected by contact resistance. In contrast, the data obtained by current measurements in the field-effect transistor configuration are strongly affected by nature of the contacts formed between the channel and electrodes. For example, single-wall carbon nanotubes contacted by Au or Pd electrodes show a p-type gate effect,[28] whereas the nanotubes contacted by a metal with low work function (e.g., Sc) show an n-type gate effect due to more efficient electron injection.[29] PbSe nanocrystal solids show p-type gate effect (Figure 4b), which is also expected from comparison of the work function and ionization potential of Au and bulk PbSe (Figure 4d). Alternatively, a positive thermopower shows that the Fermi level in a PbSe nanocrystal solid is close to the $1S_h$ quantum-confined state and that the nanocrystal array is p-doped. The detailed understanding of electronic doping and conduction mechanism in nanocrystal solids requires further study; a plausible hypothesis could be the presence of surface states behaving as shallow hole acceptors. These states are probably associated with undercoordinated or oxidized surface Se atoms which are known to create the acceptor states in bulk PbSe.[30] An alternative explanation could be the direct hopping between localized midgap surface states. From general considerations, observed hole mobilities (~0.1 cm^2/Vs) are somewhat too high for the hopping between trap states with localized wave functions that are separated by a dielectric medium. To gain a better understanding of the conduction in hydrazine-treated PbSe nanocrystal solids, we measured the temperature dependence for low-bias conduction (V_{DS} < 200mV) in

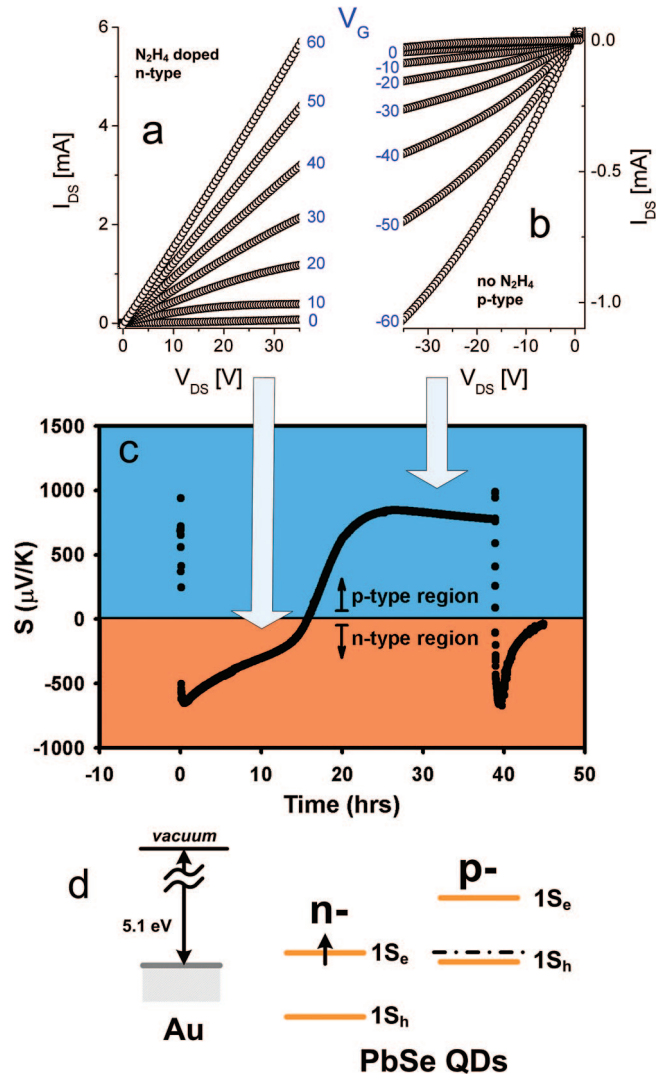

Figure 4. (a and b) Transistor measurements on 8.5-nm PbSe nanocrystal solids: plots of the current between drain and source electrodes (I_{DS}) versus drain−source voltage (V_{DS}), as a function of gate voltage (V_G). Device channel length is 10 μm, width 3000 μm, and the thickness of SiO_2 gate dielectric is 100 nm. In the presence of hydrazine, the nanocrystal solid exhibits an n-type gate effect (a) whereas removal of hydrazine in vacuum switches the device to a p-type gate effect (b). (c) Monitoring of the thermopower of a PbSe nanocrystal solid during hydrazine addition/removal (nanocrystal diameter ~9.2 nm, film thickness ~500 nm). At t = 0 h, the sample had a steady-state thermopower of 685 μV/K. A few drops of 1 M hydrazine in acetonitrile were added at t = 0 h and t = 39 h. With the addition of hydrazine, the PbSe nanocrystal solid switches from p-type ($S > 0$) to n-type ($S < 0$). See the text for more detail. (d) Energy diagram proposed for PbSe nanocrystal solid in contact with Au electrodes on the basis of combined transport and thermopower measurements.

N_2H_4-treated 7.2-nm PbSe nanocrystal solids. In the 200−310 K temperature range, the film conduction is well described by activated transport with the activation energy E_A. We found that E_A strongly depends on the applied gate voltage (V_G), varying from 200 meV (V_G = 40V) down to 85 meV (V_G = 0V) and 28 meV (V_G = −40V). Following the analysis by Mentzel et al., we estimate the depth of the acceptor states as ~50−70 meV at room temperature.[30] Thermal energy is required to generate a hole in the

nanocrystal from the acceptor state providing the mobile carrier in the $1S_h$ state. For a 60-meV-deep trap, the ionization probability at room temperature is about 10^{-1}. The DOS at the Fermi energy can be estimated as $\mathrm{DOS}(E_F) = C_i/es\,(\Delta E_F/\Delta V_G)^{-1}$ where C_i is the capacitance of the gate dielectric per unit area, s is the screening length in the nanocrystal solid, and e is the electron charge.[30] For 100-nm-thick SiO_2 gate dielectric $C_i \sim 3.4 \times 10^{-8}$ F cm^{-2}. $\Delta E_F/\Delta V_G \sim 3.1 \times 10^{-3}$ eV V^{-1} was obtained from the dependence of the activation energy on V_G. The possibility to efficiently operate the 35-nm-thick transistor channel in the depletion mode[22] shows that the screening length s is as at least 20 nm. These parameters yield $\mathrm{DOS}(E_F) < 3 \times 10^{19}$/eV cm^{-3} at $V_G = 0$V, that is, less than 0.5 electronically active acceptor states per nanocrystal and more than an order of magnitude lower than the DOS associated with S-type quantum-confined orbitals. The localization length, a, for midgap states is small ($\sim$1 nm) compared to that for S states ($\sim$nanocrystal radius, $\sim$3.6 nm). The probability of hopping between two states with similar energy is proportional to $P \sim \exp(-2d/a)$ where d is the hopping distance.[31] For $d \sim 8$ nm, which is a reasonable estimate for our nanocrystal solid, the probability of hopping between localized midgap states should be $\sim$5 orders of magnitude lower than the hopping probability for more-delocalized S states. These arguments seem to strongly support the transport through quantum-confined orbitals, not through the surface states.

To control the p-type doping level, we exposed a film of 6.4-nm PbSe nanocrystals to oxygen, which is a well-known p-dopant of bulk lead chalcogenides.[32] After the exposure, we observed an increase in the conductivity of PbSe nanocrystal film by about 1 order of magnitude (Figure S2 from the Supporting Information) accompanied with a decrease in thermopower from 760 to 440 μV/K (Figure S3 from the Supporting Information). After exposure to oxygen the nanocrystal solid showed weak gating and electrical measurements alone could not separate the conductivity increase due to changes of carrier mobility and/or doping level. The decrease in thermopower points to a shifting of the Fermi Energy closer to the $1S_h$ state due to the doping effect.

We also used thermopower measurements to study the characteristics of n-type surface charge-transfer doping of PbSe nanocrystals with hydrazine. Thermopower was monitored continuously as the relative amount of hydrazine in a nanocrystal thin film was varied. This experiment is depicted in Figure 4c. At $t = 0$ h, the sample had a steady-state thermopower of $\sim$685 μV/K, and a few drops of 1 M hydrazine in acetonitrile are placed on the film. The droplets evaporate after a few minutes, and a sharp transition from p-type ($S > 0$) to n-type ($S < 0$) is observed simultaneously. A slow transition back to p-type is observed over the course of many hours. We attribute this slow transition to evaporation of hydrazine from the nanocrystal film. These results conclusively show that n-doping of PbSe nanocrystal solids is determined by hydrazine adhered to the nanocrystal surface. The n-type doping occurs through the formation of charge-transfer complex between the nanocrystal and hydrazine molecules. Reversible behavior is demonstrated when we repeat the hydrazine treatment at $t = 39$ h. The transistor measurements on similarly treated PbSe nanocrystal films show n-type gate effects in the presence of hydrazine (Figure 4a), slowly switching to ambipolar and, finally, p-type gate effect after removal of hydrazine (Figure 4b). Because thermopower measurements are open circuit, they remove the possibility of the effects associated with nonideal contact behavior. Figure 4c also shows that hydrazine-doped PbSe nanocrystal solids can reach large negative thermopowers (ca. -650 μV/K), considerably exceeding values reported for n-PbSe.[32]

This works demonstrates that PbSe nanocrystal solids exhibit a significant thermopower enhancement of several hundred microvolts per Kelvin relative to bulk PbSe. This can be attributed to the sharp peaks in the electronic DOS of nanocrystal solids. Tunability of thermopower via changes in nanocrystal size has also been demonstrated. If the electrical conductivity can be improved, then these materials represent an emerging class of inexpensive and scalable thermoelectric materials. This can be done by either increasing the carrier concentration or improving mobility. Increasing carrier concentration generally results in a decrease in thermopower, but could enhance ZT up until a maximum S^2n is reached. This maximum value has not been achieved in this work and remains unknown. A more-promising route to improve ZT is to improve mobility (e.g., reduce carrier scattering). To compete with commercial thermoelectric materials, the carrier mobility in nanocrystal solids should be increased by at least $2-3$ orders of magnitude. Furthermore, if the reduction in carrier scattering has a favorable energy dependence, then the thermopower could be enhanced due to energy-filtering as in ref 26. In this ideal case, electrical conductivity and thermopower could be enhanced simultaneously. Colloidal nanocrystals embedded in a host material would be an interesting system that may exhibit a reduction in carrier scattering.

Acknowledgment. We acknowledge the support of the Division of Materials Sciences and Engineering, Office of Basic Energy Sciences, DOE. We thank the UC Berkeley Microfabrication Laboratory for the use of their facilities. R.Y.W. gratefully acknowledges a NSF IGERT fellowship. Work at the Molecular Foundry was supported by the U.S. Department of Energy under Contract No. DE-AC02-05CH11231. D.V.T. acknowledges NSF MRSEC program under Award No. DMR-0213745.

Supporting Information Available: Materials and methods and supplementary figures. This material is available free of charge via the Internet at http://pubs.acs.org.

References

(1) Chen, G.; Dresselhaus, M. S.; Dresselhaus, G.; Fleurial, J. P.; Caillat, T. *Int. Mater. Rev.* **2003**, *48*, 45–66.
(2) Dresselhaus, M. S.; Chen, G.; Tang, M. Y.; Yang, R. G.; Lee, H.; Wang, D. Z.; Ren, Z. F.; Fleurial, J. P.; Gogna, P. *Adv. Mater.* **2007**, *19*, 1043–1053.
(3) Hicks, L. D.; Dresselhaus, M. S. *Physical Review B* **1993**, *47*, 16631–16634.
(4) Hicks, L. D.; Dresselhaus, M. S. *Physical Review B* **1993**, *47*, 12727–12731.

(5) Hicks, L. D.; Harman, T. C.; Dresselhaus, M. S. *Appl. Phys. Lett.* **1993**, *63*, 3230–3232.
(6) Boukai, A. I.; Bunimovich, Y.; Tahir-Kheli, J.; Yu, J. K.; Goddard, W. A.; Heath, J. R. *Nature* **2008**, *451*, 168–171.
(7) Harman, T. C.; Taylor, P. J.; Walsh, M. P.; LaForge, B. E. *Science* **2002**, *297*, 2229–2232.
(8) Hochbaum, A. I.; Chen, R. K.; Delgado, R. D.; Liang, W. J.; Garnett, E. C.; Najarian, M.; Majumdar, A.; Yang, P. D. *Nature* **2008**, *451*, 163–U5.
(9) Hsu, K. F.; Loo, S.; Guo, F.; Chen, W.; Dyck, J. S.; Uher, C.; Hogan, T.; Polychroniadis, E. K.; Kanatzidis, M. G. *Science* **2004**, *303*, 818–821.
(10) Venkatasubramanian, R.; Siivola, E.; Colpitts, T.; O'Quinn, B. *Nature* **2001**, *413*, 597–602.
(11) Franchi, S.; Trevisi, G.; Seravalli, L.; Frigeri, P. *Prog. Cryst. Growth Charact. Mater.* **2003**, *47*, 166–195.
(12) Murray, C. B.; Kagan, C. R.; Bawendi, M. G. *Annu. Rev. Mater. Sci.* **2000**, *30*, 545–610.
(13) Wise, F. W. *Acc. Chem. Res.* **2000**, *33*, 773–780.
(14) Mahan, G. D.; Sofo, J. O. *Proc. Natil. Acad. Sci. U.S.A.* **1996**, *93*, 7436–7439.
(15) Humphrey, T. E.; Linke, H. *Phys. Rev. Lett.* **2005**, *94*, 096601.
(16) Chen, G. *Nanoscale Energy Transport and Conversion*; Oxford: New York, 2005.
(17) Kim, W.; Wang, R.; Majumdar, A. *Nano Today* **2007**, *2*, 40–47.
(18) Prasher, R. *Physical Review B* **2006**, *74*, 165413.
(19) Wang, R. Y.; Segalman, R. A.; Majumdar, A. *Appl. Phys. Lett.* **2006**, *89*, 173113.
(20) Vanmaekelbergh, D.; Liljeroth, P. *Chem Soc Rev* **2005**, *34*, 299–312.
(21) Yu, D.; Wang, C. J.; Wehrenberg, B. L.; Guyot-Sionnest, P. *Phys. Rev. Lett.* **2004**, *92*, 216802.
(22) Talapin, D. V.; Murray, C. B. *Science* **2005**, *310*, 86–89.
(23) Ben-Porat, C. H.; Cherniavskaya, O.; Brus, L.; Cho, K. S.; Murray, C. B. *J. Phys. Chem. A* **2004**, *108*, 7814–7819.
(24) Lazarenkova, O. L.; Balandin, A. A. *J. Appl. Phys.* **2001**, *89*, 5509–5515.
(25) Abrams, H.; Tauber, R. N. *J. Appl. Phys.* **1969**, *40*, 3868.
(26) Heremans, J. P.; Thrush, C. M.; Morelli, D. T. *Phys. Rev. B* **2004**, *70*, 115334.
(27) Rogacheva, E. I.; Tavrina, T. V.; Nashchekina, O. N.; Grigorov, S. N.; Nasedkin, K. A.; Dresselhaus, M. S.; Cronin, S. B. *Appl. Phys. Lett.* **2002**, *80*, 2690–2692.
(28) Javey, A.; Guo, J.; Wang, Q.; Lundstrom, M.; Dai, H. J. *Nature* **2003**, *424*, 654–657.
(29) Zhang, Z. Y.; Liang, X. L.; Wang, S.; Yao, K.; Hu, Y. F.; Zhu, Y. Z.; Chen, Q.; Zhou, W. W.; Li, Y.; Yao, Y. G.; Zhang, J.; Peng, L. M. *Nano Lett.* **2007**, *7*, 3603–3607.
(30) Mentzel, T. S.; Porter, V. J.; Geyer, S.; MacLean, K.; Bawendi, M. G.; Kastner, M. A. *Phys. Rev. B* **2008**, *77*, 075316.
(31) Mott, N. F. *Conduction in Non-Crystalline Materials*; Oxford: New York, 1993.
(32) Rogacheva, E. I.; Tavrina, T. V.; Grigorov, S. N.; Nashchenkina, O. N.; Volobuev, V. V.; Fedorov, A. G.; Nasedkin, K. A.; Dresselhaus, M. S. *J. Electron. Mater.* **2002**, *31*, 298–303.

NL8009704